Arabian Journal of Chemistry (2023) **16**, 104424

King Saud University

Arabian Journal of Chemistry

www.ksu.edu.sa
www.sciencedirect.com

ORIGINAL ARTICLE

Accelerated degradation of groundwater-containing malathion using persulfate activated magnetic Fe_3O_4/graphene oxide nanocomposite for advanced water treatment

Maryam Dolatabadi [a,b], **Tomasz Świergosz** [c], **Chongqing Wang** [d], **Saeid Ahmadzadeh** [e,f,*]

[a] *Student Research Committee, Kerman University of Medical Sciences, Kerman, Iran*
[b] *Environmental Science and Technology Research Centre, Department of Environmental Health Engineering, School of Public Health, Shahid Sadoughi University of Medical Sciences, Yazd, Iran*
[c] *Department of Chemical Technology and Environmental Analysis, Faculty of Chemical Engineering and Technology, Cracow University of Technology, Kraków, Poland*
[d] *School of Chemical Engineering, Zhengzhou University, Zhengzhou 450001, China*
[e] *Pharmaceutics Research Centre, Institute of Neuropharmacology, Kerman University of Medical Sciences, Kerman, Iran*
[f] *Pharmaceutical Sciences and Cosmetic Products Research Centre, Kerman University of Medical Sciences, Kerman, Iran*

Received 17 September 2022; accepted 10 November 2022
Available online 15 November 2022

KEYWORDS

Pesticide;
Persulfate;
Magnetic Fe_3O_4/Graphene oxide nanocomposite;
Groundwater;
Response Surface Methodology;
Advanced oxidation processes

Abstract Malathion (MT) is a widely used organophosphate insecticide with a broad spectrum. MT residues in the environment even at low concentrations can have adverse effects on humans, plants, animals, and ecosystems. In this study aimed to investigate the MT degradation yield from groundwater using persulfate activated magnetic Fe_3O_4/graphene oxide nanocomposite (PS/Fe_3O_4-GO MNCs). Thus, the effects of MT concentration, the dosage of PS and Fe_3O_4-GO MNCs, pH value along with reaction time were investigated and further optimized applying Response Surface Method (RSM). This model equation showed a sufficient match with the measured results from the experimental data with the correlation coefficient (R^2) of 0.9819 according to the analysis of variance. For the optimal yield, MT concentration of 3.7 mg/L, PS of 2.25 mM, Fe_3O_4-GO MNCs dosage of 225 mg/L, reaction time of 22 min and pH of 4 were obtained. Moreover, for MT

* Corresponding author.
E-mail addresses: chem_ahmadzadeh@yahoo.com, saeid.ahmadzadeh@kmu.ac.ir (S. Ahmadzadeh).

Peer review under responsibility of King Saud University.

Production and hosting by Elsevier

https://doi.org/10.1016/j.arabjc.2022.104424

degradation, the estimated optimal degradation efficiency was 96.5 %. Furthermore, a distinct synergistic effect was observed upon the usage of Fe_3O_4-GO MNCs for PS activation. The MT degradation rate is generally characterized by a pseudo-first-order kinetic model. Besides, experiments with radical scavengers revealed that both $OH^{\cdot}$ and $SO_4^{\cdot-}$ radicals had significant functions in MT degradation yields, with sulphate radicals being the dominant species. Conclusively, results revealed that the PS/Fe_3O_4-GO MNCs degradation process is an effective method for remediating waters that have been polluted with MT and related pesticides.

1. Introduction

Agricultural pesticide contamination of water reservoirs presents a severe threat to aquatic ecosystems and drinking water resources. For the past 50 years, plant protection products, collectively known as pesticides, have been an integral part of the balanced production of quality food and fibre (Sawinska et al., 2020). A prominent leadership in controlling weeds (herbicides), insects (insecticides), and plant diseases that affect the growth, yield, and marketability of crops has established the pesticide industry as a significant economic contributor in the worldwide marketplace (Popp et al., 2013). At the same time, the ubiquitous agricultural and non-agricultural utilization of pesticides has led to the residual distribution of pesticides in several environmental segments (Carvalho, 2017; Mahmoodi et al., 2021). Traces of the chemicals are regularly found in surface water and, over time, groundwater, and the primary source of drinking water around the world (Sharma and Bhattacharya, 2017). The quantity of these contaminants is sometimes reported as being below regulatory limits in water (0.1–0.5 μg/L) (Bray et al., 2021). Nevertheless, pesticide contamination of water has been claimed to be a global problem, in addition, and even more so, drinking water that has high amounts of toxins has very negative and unfavorable impacts on human population health (Rasheed et al., 2019).

Malathion (MT) (Diethyl 2-[(dimethoxyphosphorothioyl)sulfanyl] butanedioate) is a broad-spectrum, extremely toxic organophosphorus insect repellent, registered in 1956 (Chai et al., 2021), and is employed extensively in agricultural science, industry and public health to kill ants, aphids, bagworms, beetles, cotton leaf worms, insects, lice, mosquitoes, etc. by inhibiting the cholinesterase enzyme (Sharma et al., 2020). Thus, it is rapidly and efficiently absorbed by all routes, including the gastrointestinal tract, lungs, mucosa, and skin, at the same time, causing blurred vision, excessive salivation, headache, dizziness, nausea, and vomiting due to the active metabolite malaoxon (a metabolic product of MT) (Dikshith and Diwan, 2003), this metabolite is 61 times more toxic than MT. It also affects the nervous system, adrenal glands, immune system, liver and has carcinogenic implications (ur Rahman et al., 2021). Beyond that, it is toxic to birds, fish, other water invertebrates, and honeybees (DiBartolomeis et al., 2019). Consequently, as a result of the harmful consequences of pesticides in the natural environment and their potentially harmful health outcomes (Bray et al., 2021), many strict regulations and directives have been introduced to monitor the release of pesticides into the natural environment (Borsuah et al., 2020). Therefore, there are many researchers concerned with the removal of MT from aquatic media (Wang et al., 2021). A selection of techniques have been working for this purpose, including physical methods (membrane filters, sand filters) (Hedegaard and Albrechtsen, 2014; Mosleh-Shirazi et al., 2021), biological methods (biological rotary reactor, membrane bioreactor) (Srivastava et al., 2021), and chemical methods (photocatalytic oxidation, flocculation and coagulation) (da Costa Filho et al., 2016). However, there are challenges associated with some of these methods including high energy requirements to operate the process, large amounts of chemicals involved, generation of toxic by-products, high operating and/or capital costs, disposal and non-selectivity issues. The advanced oxidation processes (AOPs), generally with the participation of hydroxyl radicals ($^{\bullet}OH$) with a high redox potential (1.8–2.7 V), are widely reported for the elimination of many organic pollutants. Sulphate radical ($SO_4^{\cdot-}$) with a redox potential of about 2.6 V, has received broad attention in the field of organic pollutant management (Luo et al., 2021). Moreover, $SO_4^{\cdot-}$ has a more extended half-life ($t_{1/2} = 30 - 40\,\mu s$) in contrast to $^{\bullet}OH$ ($t_{1/2} = 1\,\mu s$), a broad operational pH range that makes for better mass transfer and contact of $SO_4^{\cdot-}$ with contaminants. However, it has always higher selectivity in comparison to $^{\bullet}OH$, $SO_4^{\cdot-}$ and thus it can be employed for rapid reaction with specific functional groups via electron transfer (Hussain et al., 2017). Generally, $SO_4^{\cdot-}$ has the potential to be produced from the initiation of persulfate (by bases, ultrasound, UV light, heat, metal ions (*e.g.*, Fe^{2+}, Co^{2+}, Cu^{2+}), and metal oxides (Fe_3O_4, CuO) (Wu et al., 2018). For PS activation, Fe_3O_4 magnetic nanoparticles (Fe_3O_4-MNPs) were selected as suitable heterogeneous catalysts due to their relatively wide availability and specific structure, easy separation/reuse, and environmental friendliness. On the other hand, the oxidation of PS with Fe_3O_4-MNPs is limited by relatively low catalytic efficiency, low oxidant utilization capacity, and incomplete degradation rate of organic compounds (Bavykina et al., 2020; Dehghani et al., 2022). Monolayers of carbon atoms with a tightly packed honeycomb lattice have made graphene of great interest among nanotechnology researchers in recent years. Graphene has the potential to enhance the electron charge transfer rate and the number of chemical molecules adsorbed on the surface through π-π interactions. More recently, Fe_3O_4/graphene oxide (GO) magnetic nanocomposites have received high interest in terms of promoted transfer and adsorption properties (Asadzadeh Patehkhor et al., 2021; Hussain et al., 2012).

In this research, Fe_3O_4-graphene oxide (GO) magnetic nanocomposites (Fe_3O_4-GO MNCs) were synthesized and employed to activate PS for MT degradation. This study aimed to prepare and characterize Fe_3O_4-GO MNCs nanocomposites. Moreover, since several factors are involved in the process, including MT concentration, the dosage of PS and Fe_3O_4-GO MNCs, pH solution, and reaction time, an advanced experimental proposal as response surface methodology (RSM) was employed over the conventional single variable study to systematically investigate the most desirable MT degradation parameters using PS/Fe_3O_4-GO MNCs, and propose mechanisms for MT activation and degradation.

2. Materials and methods

Among the chemical reagents, malathion ($C_{10}H_{19}O_6PS_2$, >99.0 %) and graphite were purchased from Sigma Aldrich, Germany. Potassium persulfate ($K_2S_2O_8$, >99.0 %), ammonium persulfate ($(NH_4)_2S_2O_8$, ≥98.0 %), sodium persulfate ($Na_2S_2O_8$, ≥98.0 %), sodium thiosulfate ($Na_2S_2O_3$, >99.0 %), sodium hydroxide (NaOH, ≥98.0 %), hydrogen peroxide (H_2O_2, 30 % w/w), potassium permanganate ($KMnO_4$, ≥99.0 %), ferric chloride ($FeCl_3$, ≥99.9 %), sulfuric acid (H_2SO_4, ≥99.9 %), ethylene glycol ($C_2H_6O_2$, ≥99.0 %), sodium acetate ($C_2H_3NaO_2$, ≥99.9 %), ethanol (C_2H_5OH, ≥99.9 %), tertiary butanol ($C_4H_{10}O$, ≥99.5 %) and methanol

(CH_3OH, HPLC grade, ≥99.9 %) were obtained from Merck Company, Germany. All chemicals were at least analytical grade and were used as received. Moreover, all solutions were prepared in distilled water obtained from Abban Company.

2.1. Preparation and characterization of Fe_3O_4-GO MNCs

2.1.1. Graphene oxide (GO) preparation

From natural graphite, graphene oxide (GO) was fabricated by the Hummers method with some small modifications (Zaaba et al., 2017). Towards that, place 2 g of powdered natural graphite in a 250 mL beaker, then gradually add 1 g of $NaNO_3$ and 46 mL of H_2SO_4 while stirring in an ice bath. Thereafter, 6 g of $KMnO_4$ was slowly added to the beaker with stirring while maintaining the temperature below 20 °C. After 5 min the ice bath was removed and the system was heated to 35 °C for 30 min, then 92 mL of water was slowly added and vortexed for an additional 15 min. Subsequently, to reduce residual $KMnO_4$, add 80 mL of 60 °C hot water and 3 % H_2O_2 in water until no more visible bubbles are visible. Finally, the system was centrifuged at 7200 rpm for 10 min, and the resulting powder was washed with warm demineralized water until the pH of the upper suspension reached 7. However, after cleaning the black residue, the resulting tan powder was dispersed in ultrapure water and sonicated with gentle sonication for 15 min to form homogeneous suspensions of varying concentrations. GO powder was received by lyophilization of the suspension (Han et al., 2011).

2.1.2. Preparation of Fe_3O_4-GO MNCs

After the typical synthesis, the pre-treated GO (0.5 g) was fractionated by sonication in 80 mL of ethylene glycol over 3 h. Next, 1.6 g $FeCl_3$-$6H_2O$ and 3.2 g sodium acetate were dissolved in the ethylene glycol GO solution at ambient temperature. After vortexing for approximately 30 min, the solution was transferred to a 100 mL Teflon-lined stainless steel autoclave and kept at 200 °C for 6 h before naturally cooling to ambient temperature. Finally, the black pellet was centrifuged, washed several times with ethanol, and dried in a vacuum oven at 60 °C (Ai et al., 2011).

2.2. Experimental procedures

A 300 mL sealed Erlenmeyer flask with a rotary shaker (200 rpm, 20 ± 2 °C) was used in all experiments. The reactions involved were initiated by adding the indicated amount of Fe_3O_4-GO-MNCs to 250 mL of a mixed solution containing MT and PS. Moreover, to determine the effect of different parameters on MT degradation, several sets of experiments were performed. The solution pH was adjusted operating NaOH or H_2SO_4. To identify the influence of the reactive species in PS activated by Fe_3O_4-GO MNCs process (PS/ Fe_3O_4-GO MNCs), ethanol (EtOH) and tertiary butanol (TBA) were utilized as radical scavengers. Also, to verify the ability to reuse Fe_3O_4-GO MNCs, the MNCs were collected with a magnet and washed with Milli-Q water after each run, followed by reuse with the addition of fresh PS and MT. All experiments were performed in triplicate, and the standard deviation of all experiments was given. Collect 2 mL samples at regular intervals and pass through a 0.45 μm PTFE filter. Then 10 μL of 1 M $Na_2S_2O_3$ was added to quench the reaction. The filtered solution was analysed for MT concentration.

The detection of MT residual in samples after the treatment process were further validated by using High-performance liquid chromatography (HPLC) (KNAUER HPLC system model Smartline, Germany) having a UV detector with 220 nm wavelength. For this purpose, a Reliant C18 column (250 × 4.6 mm) was used and maintained at a constant column temperature of 40 °C. A solution of acetonitrile and water (75:25) was used as eluent at a flow rate of 1 mL min^{-1} with a retention time of 25 min. The structure and morphology of the Fe_3O_4-GO MNCs were characterized by Field Emission scanning electron microscopy (FE-SEM, LEO-Germany).

2.3. Statistical model

Response surface methodology (RSM) stands for statistically identifying important factors (independent variables) in a model and generating a response surface model, which is used to predict outcomes by providing mathematical equations. In this study, experiments were designed using Design Expert version 11 software.

For this purpose, four independent variables are considered in the experimental design as follows concentration of MT, the dosage of PS, the dosage of Fe_3O_4-GO MNCs and reaction time. The dependent variable (response) is the degradation efficiency of MT. Each of the independent variable (X_1, X_2, X_3, and X_4) was varied numerically over five levels and coded as -α,-1, 0, +1 and + α Analysis of variance (ANOVA) and regression analysis were performed to determine the statistical significance of the model conditions, with regression correlation fit between experimental data and independent variables. Assuming that the changes in Y, (MT degradation efficiency) are consistent with a second order equation of the form Eq.1:

$$Y = \beta_0 + \sum_{i=1}^{n} \beta_i X_i + \sum_{i=1}^{n} \beta_{ii} X_i^2 + \sum_{i=1}^{n-1} \sum_{j=i+1}^{n} \beta_{ij} X_i X_j \quad (1)$$

Y denotes the response value estimated by the model, β_0 is a constant, β_i denotes that the shift value is linear, β_{ii} is quadratic, and β_{ij} is the regression coefficient of correlation. X_i and X_j denote the coded independent variables. The validity of the model was determined by model summary, no-fit model test, and coefficient of determination (R^2) analysis The terms were removed from the initial model for all statistically insignificant terms (*p-value* > 0.05), and the empirical data were re-fitted only for significant (*p-value* < 0.05) result variables to obtain the final reduced model.

3. Results and discussion

3.1. Characterization of Fe_3O_4-GO MNCs catalyst

For the purpose of investigating the morphology and structure of the catalyst, there was FE-SEM image taken for the fabricated Fe_3O_4-GO MNCs and shown in Fig. 1-**(A)**. In addition, GO distributed between Fe_3O_4 nanoparticles can prevent the aggregation of Fe_3O_4 nanoparticles to some extent resulting in a potentially beneficial effect on the reaction Even more relevant, after a long sonication time during FE-SEM sample

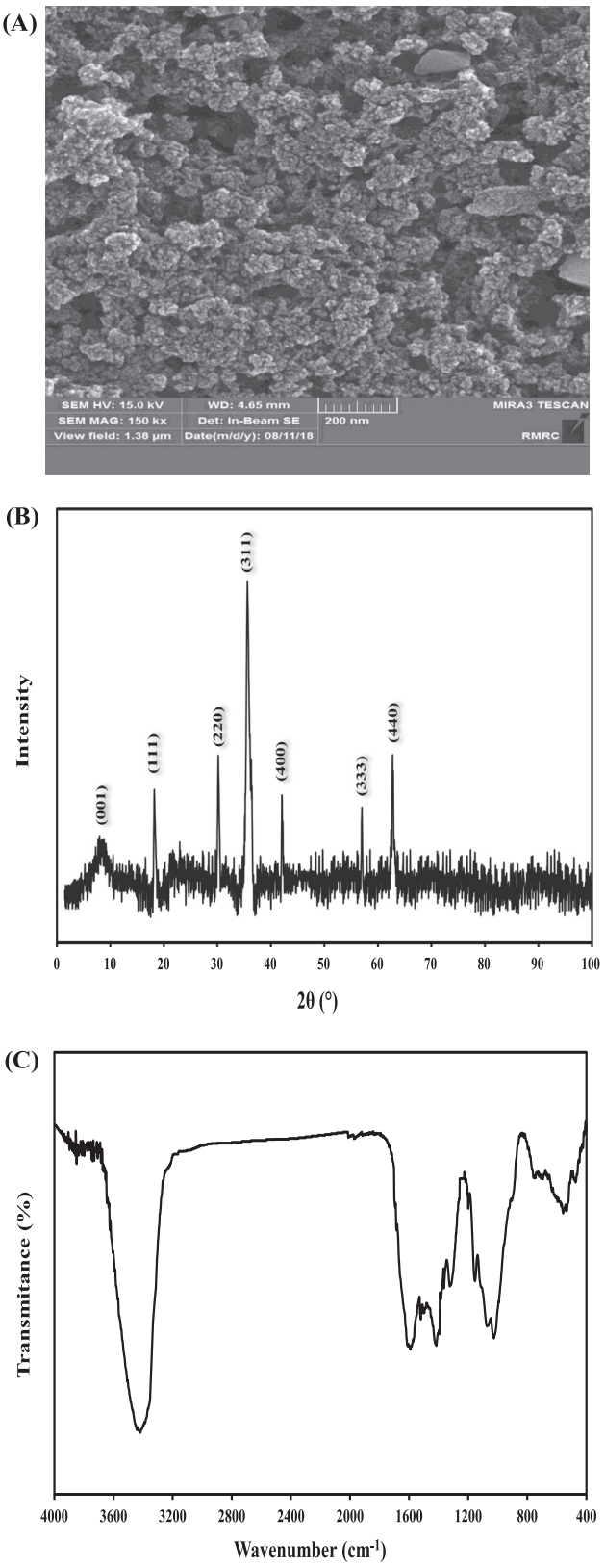

Fig. 1 **(A)** The FE-SEM image, (**B**) XRD pattern, and (**C**) FTIR spectra of Fe_3O_4-GO MNCs.

preparation, the Fe_3O_4 nanoparticles were still tightly attached on the GO surface with high density, suggesting a strong interaction between Fe_3O_4 nanoparticles and GO. Also, it shows that the nanoparticles are agglomerated due to magnetic dipolar interactions between the magnetite nanoparticles.

The crystalline structure of Fe_3O_4-GO MNCs was identified with XRD technique. The XRD pattern of Fe_3O_4-GO MNCs is shown in Fig. 1-**(B)**. The peaks at 2θ values of 17.9° (111), 30.7° (220), 35.9° (311), 42.8° (400), 57.3° (422), and 63.1° (511) are in agreement with standard XRD data for an inverted Fe_3O_4 spinel structure with lattice constants of θ = 8.397°A (JCPDS file no. 19–0629). Computations with the Scherrer equation reveal an 18 nm equivalent particle size, as confirmed by FE-SEM. Also, the Fe_3O_4 diffraction peaks are wider, suggesting that the crystal sizes are quite small for Fe_3O_4 particles. Moreover, a diffraction peak marked by a very slight oval shape at 2θ = 9.7° belongs to (001) crystal of GO. The obtained results correlate well with the previous studies (Kassaee et al., 2011; Yao et al., 2012).

In Fig. 1-**(C)**, the fourier transform infrared spectroscopy (FTIR) spectra of Fe_3O_4-GO MNCs have been provided. The intense peaks at 3427 cm^{-1} is associated with the stretching of O—H groups. The peak at 1638 cm^{-1} (aromatic C=C) can be attributed to the skeletal vibrations of the unoxidized graphite domains (Kassaee et al., 2011). The peak at 1363 cm^{-1} relates to the bending absorption of carboxyl group O=C (Amani et al., 2022), while the two characteristic absorption peaks of Fe-O in Fe_3O_4 nanoparticles appear at 572 cm^{-1} and 628 cm^{-1}. The characteristic peaks at 1571 and 1251 cm^{-1} indicate the interaction of carbonyl and epoxy groups of GO and Fe on the surface of magnetic particles, and establish the binding of Fe_3O_4 nanoparticles to GO (Umar et al., 2020).

3.2. Establishment for a new MT degradation activation system

Initially, the effects of numerous PSs including $(NH_4)_2S_2O_8$, $K_2S_2O_8$ and $Na_2S_2O_8$ on MT degradation efficiency were checked, and no noticeable differences were observed between these PSs; hence, $K_2S_2O_8$ was selected for further study. Prior to an extensive study on the MT degradation yield using PS/Fe_3O_4-GO MNCs, the MT degradation yield using PS and Fe_3O_4-GO MNCs was investigated independently in control experiments. When $S_2O_8^{2-}$ or Fe_3O_4-GO MNCs were added lonely, the MT degradation yields were 2.6 % and 21 %, respectively, both of these cases were insignificant compared to the almost complete degradation yield of MT in the presence of both $S_2O_8^{2-}$ and Fe_3O_4-GO MNCs. As a result, the significant MT degradation efficiency of PS/Fe_3O_4-GO MNCs may be due to the activation of $S_2O_8^{2-}$ by Fe^{2+} dissolved from Fe_3O_4-GO MNCs (Shang et al., 2019; Zhen et al., 2018).

3.3. Developed model and effect of operational parameters

Aqueous solution pH has a major impact on oxidation processes through changes in the degree of ionization of impurities and oxidants, surface properties, and the degree of activity and solubility of reactants. Therefore, it is based on the important role of solution pH on degradation efficiency in chemical reactions, among them advanced oxidation, the efficiency of PS/Fe_3O_4-GO MNCs process for MT degradation yield from groundwater was studied at a pH range of 2–12 and the results are given in Fig. 2.

The degradation efficiency of MT showed an increasing trend from 26.7 % to 90.3 % when the pH was downregulated

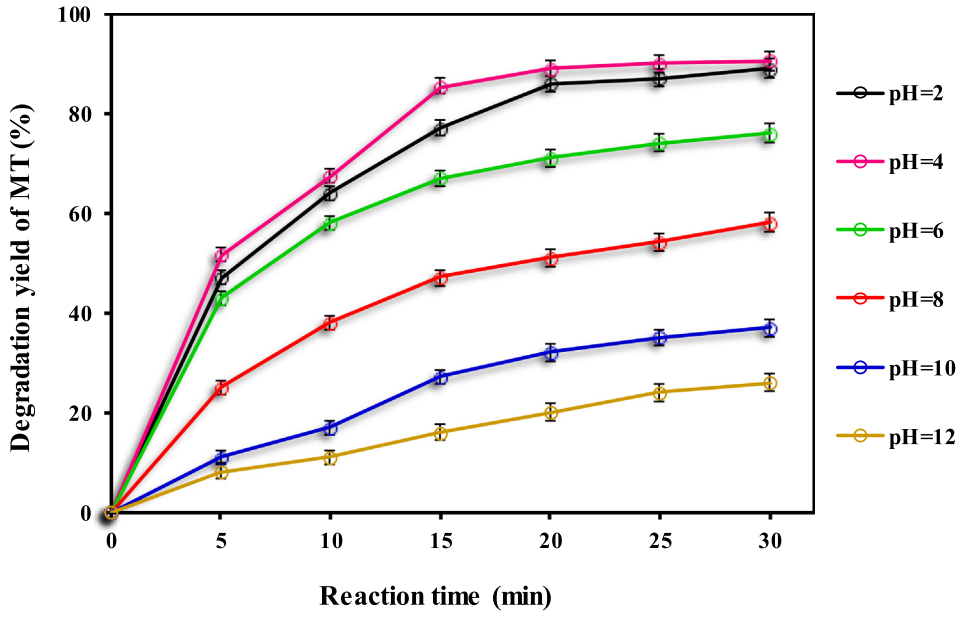

Fig. 2 Effect of pH solution for degradation yield of MT using PS/Fe_3O_4-GO MNCs process: MT concentration of 5.0 mg/L, PS dosage of 2 mM, pH of 4, and Fe_3O_4-GO MNCs dosage of 150 mg/L.

from 12 to 4. This result indicates that an acidic environment is more favourable for MT degradation than neutral and alkaline conditions. Any change in solution pH, whether below or above 4, leads to a decrease in MT degradation efficiency. Hence, the solution pH of 4 was preferred as the optimum solution pH and was applied in further experiments. If the pH is very low (strongly acidic), a large number of hydrogen ions (H^+) are present in solution, allowing them to scavenge both sulphate and hydroxyl radicals. as shown in Eqs. (2) and (3).

$$SO_4^{\cdot-} + H^+ + e^- \rightarrow HSO_4^{\cdot-} \quad (2)$$

$$OH^{\cdot} + H^+ + e^- \rightarrow H_2O \quad (3)$$

$SO_4^{\cdot-}$ mostly occurs in acidic and neutral conditions, and $OH^{\cdot}$ mostly is found in high pH conditions. Moreover, $OH^{\cdot}$ radicals can be generated from the outcomes of $SO_4^{\cdot-}$ with H_2O /OH^- (Eqs. (4) and (5)):

$$SO_4^{\cdot-} + H_2O \rightarrow OH^{\cdot-} + HSO_4^{\cdot-} \quad (4)$$

$$SO_4^{\cdot-} + OH^- \rightarrow OH^{\cdot} + SO_4^{2-} \quad (5)$$

However, the radical $SO_4^{\cdot-}$ dominates at acidic pH, but both $SO_4^{\cdot-}$ and $OH^{\cdot}$ radicals are present, and in alkaline pH and near to 12, $OH^{\cdot}$ is the dominant radical. Consequently, when PS/Fe_3O_4-GO MNCs is treated as an oxidant, corresponding to Eq. (4), including $SO_4^{\cdot-}$, $OH^{\cdot}$ is also generated. Hence, the yield decreases at high pH (Eq. (6)) due to the reaction of $SO_4^{\cdot-}$, a radical by $OH^{\cdot}$, which leads to higher consumption of $SO_4^{\cdot-}$, and subsequent decrease in MT degradation yield (Liang et al., 2020).

$$SO_4^{\cdot-} + OH^{\cdot} \rightarrow SO_4^{2-} + OH^{\cdot}\ \text{Alkaline pH} \quad (6)$$

$$OH^{\cdot} + S_2O_8^{2-} \rightarrow OH^- + S_2O_8^{\cdot} \quad (7)$$

$$OH^{\cdot} + OH^{\cdot} \rightarrow H_2O_2 \quad (8)$$

Furthermore, the reactions described in Eqs. (7) and (8) can also follow in the company of $OH^{\cdot}$ radicals at pH levels of 8 to 10 and 12, respectively. The reaction of $OH^{\cdot}$ with $OH^{\cdot}$ may result in rapid loss of $OH^{\cdot}$ in basic alkaline solution. Therefore, the decomposition efficiency of MT under alkaline conditions will be less as compared to acidic and neutral conditions. The $OH^{\cdot}$ redox potential also becomes lower under alkaline conditions (about 2.0 V), leading to a decrease in the oxidation potential of $OH^{\cdot}$ radicals (Norzaee et al., 2018).

For the optimization purpose, an experimental study on the MT degradation performance using PS/Fe_3O_4-GO MNCs process was conducted. To design the experiment, response surface methodology (RSM) was applied. Therefore, the four variables studied were MT concentration (X_1), PS dosage (X_2), Fe_3O_4-GO MNCs dosage (X_3) and reaction time (X_4). These variables and the range studied have been selected based on the literature and the results obtained in preliminary studies (Table 1). Finally, this model was designated on the basis of the high ranking order polynomials in which additional conditions were significant. Based on the MT degradation yield data shown in Table 1, a quadratic model was made using RSM since it was statistically substantial for the response (Y) for MT degradation efficiency.

In terms of coding factors, the empirical RSM model represents the interaction and importance of the variables in the direction of the response. One-factor coefficients represent the effect of only one factor, while two-factor and second-order element coefficients correspond to interactions or quadratic effects between two factors. Therefore, the final empirical formula model of the response according to the coding factor is given by Eq. (9).

$$Y(\%) = 77.75 - 6.81X_1 + 6.37X_2 + 5.56X_3 + 5.11X_4 + 4.33X_2X_3 - 5.02X_2^2 - 4.97X_3^2 \quad (9)$$

Table 1 Experimental factors and levels in the central composite design (CCD) for degradation yield of MT using PS/Fe_3O_4-GO MNCs process.

Coded Variables (X_i)	Factors (U_i)				Experimental Field					
	A = MT concentration (mg/L)					-α	−1 level	0	+1 level	+α
X_1						1	3.7	5.5	7.3	10
X_2	B = PS dosage (mM)					0.5	1.25	1.75	2.25	3
X_3	C = Fe_3O_4-GO MNCs dosage (mg/L)					50	125	175	225	300
X_4	D = Reaction time (min)					5	12.5	17.5	22.5	30
Run	**Actual values**				**Coded values**				Actual degradation	Predict degradation
	A(mg/L)	**B (mM)**	**C(mg/L)**	**D(min)**	**X_1**	**X_2**	**X_3**	**X_4**	yield of MT **(%)**	yield of MT **(%)**
1	3.7	2.25	225	12.5	−1	1	1	−1	82.6	85.7
2	3.7	2.25	125	22.5	−1	1	−1	1	76.1	76.2
3	3.7	2.25	125	12.5	−1	1	−1	−1	67.1	65.9
4	1	1.75	175	17.5	−2.5	0	0	0	93.2	94.7
5	5.5	1.75	175	17.5	0	0	0	0	79.1	77.7
6	10	1.75	175	17.5	2.5	0	0	0	62.2	60.7
7	3.7	1.25	125	12.5	−1	−1	−1	−1	62.4	61.8
8	5.5	1.75	50	17.5	0	0	−2.5	0	34.3	32.8
9	3.7	1.25	125	22.5	−1	−1	−1	1	69.3	72.1
10	7.3	1.25	225	12.5	1	−1	1	−1	49.8	50.7
11	5.5	1.75	300	17.5	0	0	2.5	0	62.2	60.6
12	3.7	1.25	225	22.5	−1	−1	1	1	71.6	74.5
13	7.3	2.25	125	12.5	1	1	−1	−1	50	52.3
14	5.5	3	175	17.5	0	2.5	0	0	63.3	62.2
15	5.5	1.75	175	30	0	0	0	2.5	92.1	90.5
16	7.3	1.25	125	22.5	1	−1	−1	1	56	58.4
17	7.3	2.25	125	22.5	1	1	−1	1	59.7	62.5
18	5.5	0.5	175	17.5	0	−2.5	0	0	32.5	30.4
19	5.5	1.75	175	17.5	0	0	0	0	78.2	77.7
20	5.5	1.75	175	17.5	0	0	0	0	80.1	77.7
21	7.3	2.25	225	22.5	1	1	1	1	80	82.3
22	5.5	1.75	175	17.5	0	0	0	0	81.8	77.7
23	5.5	1.75	175	17.5	0	0	0	0	80.7	77.7
24	5.5	1.75	175	17.5	0	0	0	0	81.3	77.7
25	7.3	1.25	225	22.5	1	−1	1	1	58.4	60.9
26	5.5	1.75	175	5	0	0	0	−2.5	62	64.9
27	3.7	1.25	225	12.5	−1	−1	1	−1	65.1	64.3
28	7.3	1.25	125	12.5	1	−1	−1	−1	47.5	48.2
29	3.7	2.25	225	22.5	−1	1	1	1	96.5	95.9
30	7.3	2.25	225	12.5	1	1	1	−1	72.7	72.1

The correlation coefficient, R^2 value, was significant to validate the elaborated model. The R^2 values for degradation yield of MT is 0.9819. It shows an overall change of 98.19 in the correlation of MT mining production between experimental and predicted values. These high R^2 values indicate that the predicted response was near the experimental value and the model is proper to connect with the experiment data. Therefore, the R^2 shows good agreement between experimental data. Fig. 3**-(A)** and **3-(B)** presents the predicted response versus actual response and the normal % probability versus externally studentized residuals for degradation yield of MT using PS/Fe_3O_4-GO MNCs process, respectively. The residuals can be seen to exhibit a normal distribution since all points were along a straight line. The residuals also revealed that the model could not be further improved through changes in the response because the data points were scattered and did not display a "sigmoidal shape" curve. However, the graphs indicated that the model presented in Equation (9) can be considered as the best suggested model for the obtained experimental data to find the optimal degradation performance of MT. Furthermore, low standard deviation values of 2.46 was obtained for the model.

The significance and contribution of independent variables and interactions were determined using graphical Pareto analysis to explain the results. This analysis determines the percentage effect of each independent variable on the dependent variable (MT degradation), based on Equation (10).

$$P_i = \frac{b_i^2}{\sum b_i^2} \times 100 (i \neq 0) \tag{10}$$

where b_i is the estimation of the principal influence of variable i. The results of the graphical Pareto analysis are illustrated in Fig. 4**-(A)**. According to this analysis, the contributions of the X_1, X_2, X_3, X_4, X_2X_3, X_2^2, and X_3^2 (significant parameters) on the MT degradation are 21.8 %, 19.1 %, 14.5 %, 12.3 %, 8.8 %, 11.8 %, and 11.6 %, respectively. According to the observations, the most important variables affecting the response rate variable are MT concentration and PS dosage. The multiple regression analysis technique in RSM to estimate the coefficients of the model for the response was applied. Furthermore, the significance and adequacy of the model were verified using ANOVA. The mean square is obtained by dividing the sum of squares of each source, model, and error variance

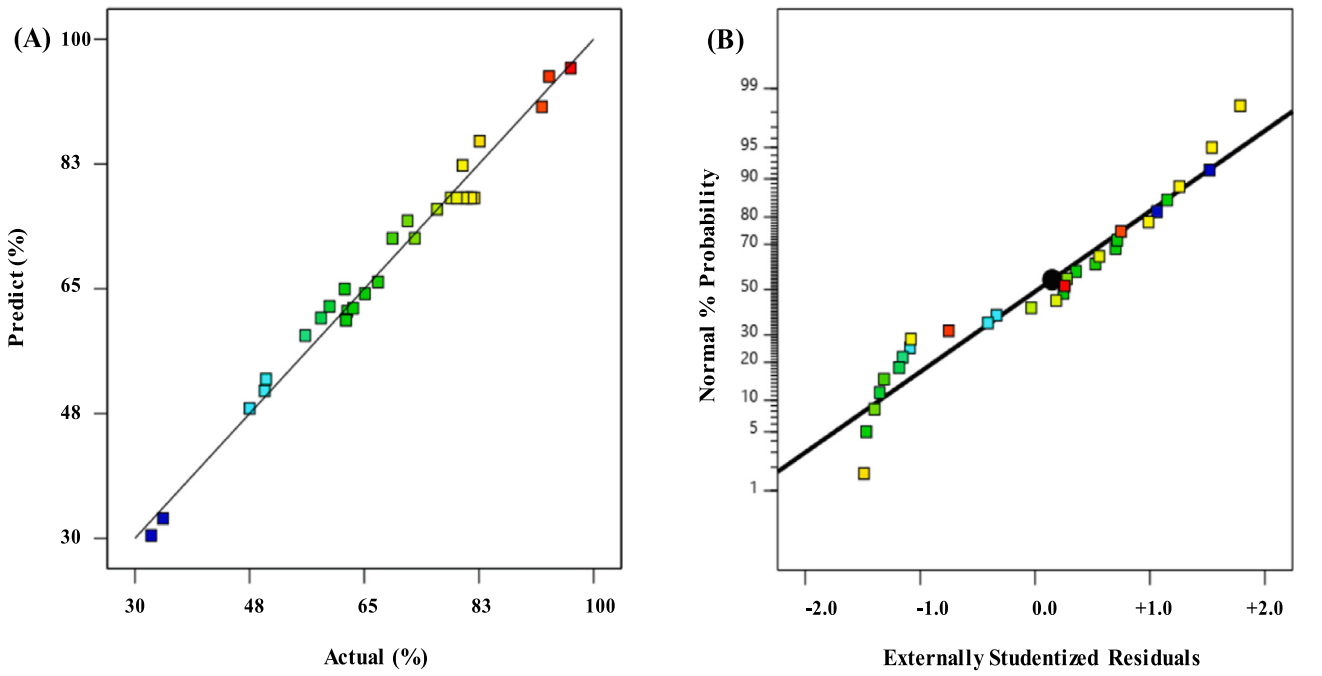

Fig. 3 **(A)** the predicted response versus actual response (**B**) the normal % probability versus externally studentized residuals for degradation of MT using PS/Fe_3O_4-GO MNCs process.

by the corresponding degrees of freedom. A low Prob > F value of < 0.05 indicates that the results are not random and that the model terms have a significant effect on the response. The analysis of variance of the quadratic model of MT degradation yield using PS/Fe_3O_4-GO-MNC process is shown in Table 2**.** From this table, a model F value of 170.14 and a Prob > F value of 0.0001 means the model is considerable.

The study of degradation yield of MT from groundwater using PS/Fe_3O_4-GO MNCs procedure at different MT concentrations was conducted in the range of 1–10 mg/L. According to Fig. 4**-(B)**, there was a significant decrease in its degradation efficiency in groundwater as the MT concentration increased. In fact, an increase in MT concentration from 1 to 20 mg/L caused reduction of efficiency of the process from 94.7 to 60.8 %. The reduction in MT degradation efficiency at higher concentrations may be due to inhibition of PS reactions at redox-active centres, reduced action of PS and Fe_3O_4-GO MNCs, leading to reduced formation of reactive species, and competition between intermediate and parent compounds in reacting with oxygen reactive radicals.

In fact, since the SO_4^{2-} radicals appear to be inert and would not be considered a type of pollutant, it should only be limited to a maximum concentration of 250 mg/L, based on the water's taste and odour as determined by the United Protection Agency. In addition to the cost of PS, it is preferable to select the lowest concentration of PS that can result in MT degradation within a given reaction time. The effect of PS concentrations (0.5 to 3 mM) on MT degradation yield was investigated (Fig. 4**-(C)**). As can be observed in Fig. 4**-(C)**, the degradation yield of MT increased with growing PS concentration. When the concentration of PS increased from 0.5 to 2 mM, the degradation yield of MT increased from 30.4 % to 86.7 %. However, when the PS concentration is higher than 2 mM, the degradation yield of MT is slightly reduced.

The reason may be that $SO_4^{\cdot-}$ is converted into $S_2O_8^{\cdot-}$ through Eqs. (11) and (12), while the oxidation potential of $S_2O_8^{\cdot-}$ is lower than that of $SO_4^{\cdot-}$.

$$SO_4^{\cdot-} + SO_4^{\cdot-} \rightarrow S_2O_8^{2\cdot-} \quad (11)$$

$$SO_4^{\cdot-} + S_2O_8^{2-} \rightarrow S_2O_8^{\cdot-} + SO_4^{2-} \quad (12)$$

Therefore, the optimal PS concentration for degradation yield of MT was found to be 2 mM in the present study.

The effect of Fe_3O_4-GO MNCs dosage on PS on MT degradation performance was investigated. Fig. 4-(D) shows the MT degradation yield as a function of PS concentration and Fe_3O_4-GO MNCs dosage in solution.

As can be seen from Fig. 4**-(D),** an enhancement of MT degradation yield is observed by increasing Fe_3O_4-GO MNCs dosage from 50 to 200 mg/L had a beneficial effect on the MT degradation efficiency. The reason for this is the increased number of active sites in Fe_3O_4-GO MNCs to react with PS, yielding more reactive sites of $SO_4^{\cdot-}$ radicals (Eq.13).

$$Fe^{2+} + S_2O_8^{2-} \rightarrow Fe^{3+} + SO_4^{2-} + SO_4^{\cdot-} \quad (13)$$

However, it is found that as the dosage of Fe_3O_4-GO MNCs had increased from 200 to 300 mg/L, MT degradation yield decreased. However, when the Fe_3O_4-GO MNCs dosage is higher than 200 mg/L, the degradation yield of MT is decreased. A possible explanation for this is (1) elevated $SO_4^{\cdot-}$ species quenching resulting from the association of $SO_4^{\cdot-}$ species alone triggered in excess of activator, and (2) increased quenching of $SO_4^{\cdot-}$ with Fe^{2+} at high activator dose through Eq.14.

$$Fe^{2+} + SO_4^{\cdot-} \rightarrow Fe^{3+} + SO_4^{2-} \quad (14)$$

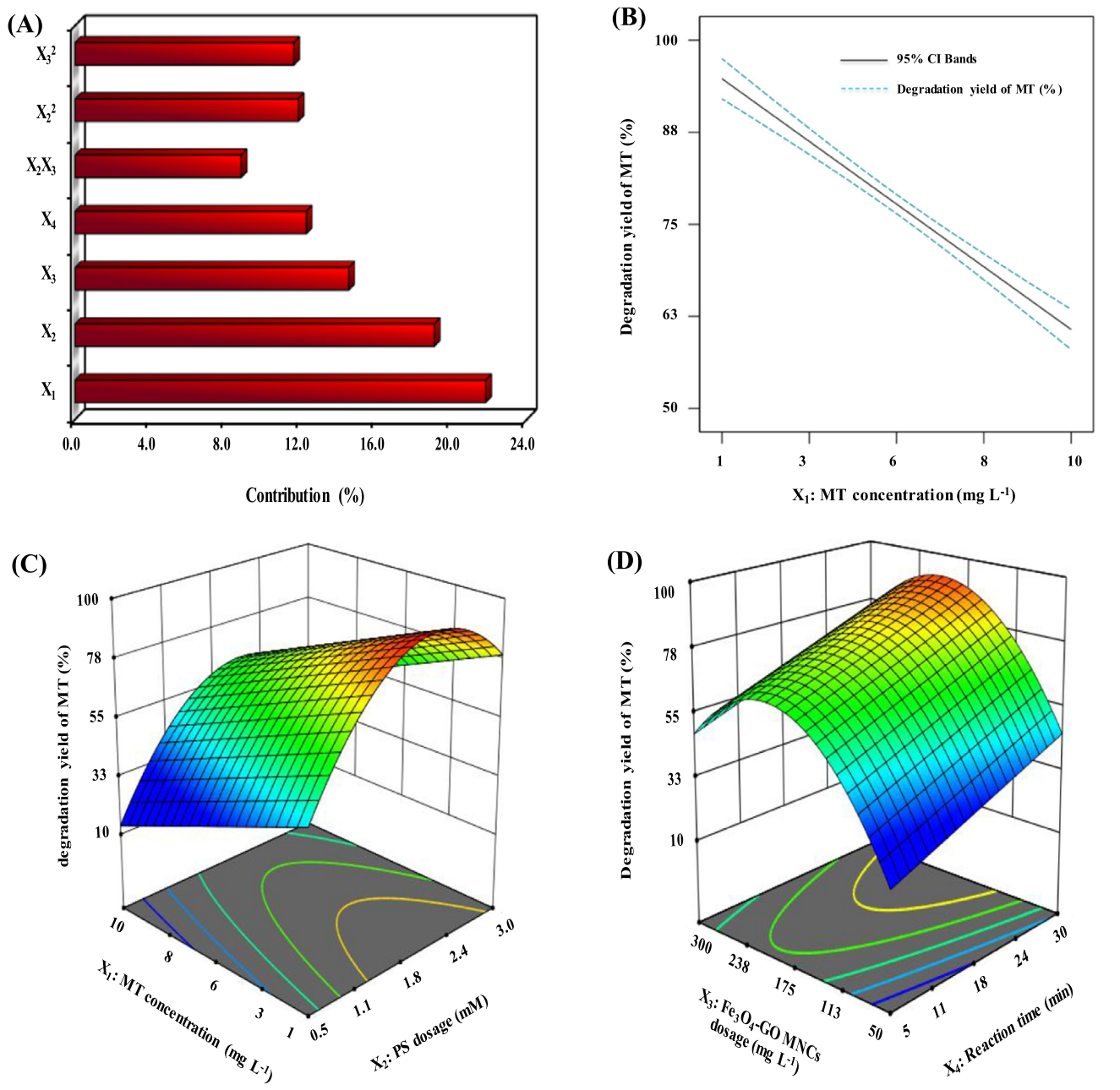

Fig. 4 **(A)** Graphical Pareto analysis of the significant operating parameters effects, (**B**) Effect of MT concentration on MT degradation yield, (**C**) Response surface plot of MT concentration & PS dosage, (**D**) Response surface plot of Fe_3O_4-GO MNCs dosage & Reaction time. (Operating parameters set at their central points of 3.7 mg/L MT concentration, PS dosage of 1.75 mM, pH of 4, Fe_3O_4-GO MNCs dosage of 175 mg/L and Reaction time of 17.5 min).

Thereupon, the MT degradation yield decreased when the Fe_3O_4-GO MNCs was added further beyond about 200 mg/L. For the control experiment, only 13.5 % MT loss was observed in the absence of Fe_3O_4-GO MNCs, indicating a low oxidation capacity of PS without using an activator.

3.4. Optimization and validation of model

With the objective to maximize the MT degradation yield using PS/Fe_3O_4-GO MNCs process, the variation of operating parameters values presents by the ramps demonstrated in Fig. 5-**(A)**. The desirability of each factor and response is shown, as well as the mixed desirability. Highlighted points illustrate optimal values for each factor or response (moving points horizontally) and how well those goals are achieved (how high the slope is). The complexity desirability of the model is 0.940, remember that the goal of optimization is to find a global solution that satisfies all objectives, desirability is just a mathematical property, not every desirability will reach a value of 1.0. A series of experiments were conducted to test the model to assess the reliability of the optimal conditions predicted by the empirical model. The experimental val-

Table 2 Analysis of variance (ANOVA) results of quadratic model to degradation yield of MT using PS/Fe_3O_4-GO MNCs process.

Source	Sum of squares	Degree of freedom (df)	Mean square	*F-value*	*p-value* prob > F
Model	7197.3	7	1028.2	170.1	< 0.0001
X_1	1321.9	1	1321.9	218.7	< 0.0001
X_2	1157.1	1	1157.1	191.4	< 0.0001
X_3	879.8	1	879.8	145.5	< 0.0001
X_4	744.3	1	744.3	123.1	< 0.0001
X_2 X_3	299.3	1	299.3	49.5	< 0.0001
X_2^2	1646.4	1	1646.4	272.4	< 0.0001
X_3^2	1609.9	1	1609.9	266.4	< 0.0001
Residual	132.9	22	6.0	–	–
Lack of Fit	123.7	17	7.2	3.9	0.0680
Pure Error	9.24	5	1.8	–	–
Cor Total	7330.3	29	–	–	–

ues were found to deviate less from the predicted values, and these results further support the validity of the model.

The optimum conditions predicted for MT degradation yield using PS/Fe_3O_4-GO MNCs process are as the MT concentration of 3.7 mg/L, PS dosage of 2.3 mM, Fe_3O_4-GO MNCs dosage of 224 mg/L, reaction time of 22 min, and pH solution of 4.0. According to the obtained results, the predicted and experimental degradation yield of 95.9 % and 96.5 % achieved in the mentioned optimum condition.

Furthermore, the accuracy of the developed polynomial model was successfully validated by performing different processing runs under a range of operating conditions and is sum-

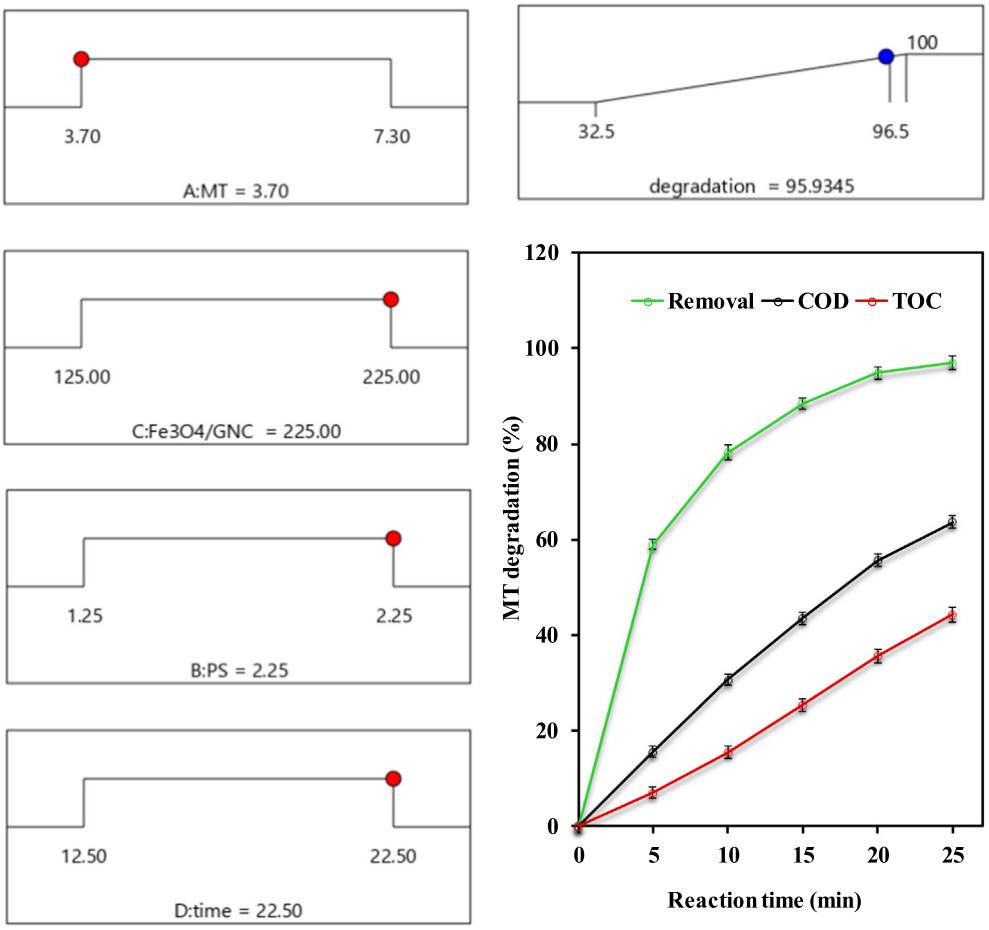

Fig. 5 (A) Ramps of numerical optimization of operating parameters values – (B) MT degradation, COD and TOC removal in the optimum condition.

marized in Table 3. From this, it can be concluded that the experimentally obtained MT degradation yields are reasonably consistent with the yields predicted by the RSM model.

3.5. Degradation kinetic

In the present work, first and second order kinetic model was used to investigate the MT degradation performance using PS/Fe_3O_4-GO MNCs process. The kinetic studies of MT degradation yield were performed in optimum condition. From the kinetic results obtained (Table 4), the correlation coefficient (R^2) of the model used was approximately 0.9965, confirming the high ability of model to fit the kinetic data of MT degradation by PS/Fe_3O_4-GO MNCs process. This is also confirmed by the strong agreement between the first-order reaction kinetics model and the experimental data from the studied process.

Table 4 Parameters of kinetic equations for the MT degradation yield.

Kinetics model	Equation	k_{app}	R^2
First order	$\ln\left(\frac{C_0}{C_t}\right) = +kt$	0.1325	0.9965
Second order	$\frac{1}{C_t} = kt + \left(\frac{1}{C_0}\right)$	0.3848	0.9050

3.6. Mechanism of MT degradation

3.6.1. Radical scavengers effect

In addition, in order to better explain the MT degradation mechanism and to identify the dominant radicals in the degradation process of PS/Fe_3O_4-GO MNCs, radical quenching experiments were performed, the results of which are shown in Fig. 6- (A). From Fig. 6-**(A)**, it is clearly seen that there was a significant decrease in MT degradation efficiency in the presence of ethanol (EtOH), benzoquinone (BQ), and tertiary butanol (TBA). However, the degradation efficiency was clearly inhibited when TBA, EtOH and BQ were added to the solution separately, and the degradation efficiencies were only 74.1 %, 27.9 % and 30.1 % for BQ, EtOH and TBA, respectively. BQ, EtOH, and TBA are established to determine the impact of $OH^{\cdot}$ and $SO_4^{\cdot-}$ radicals at different levels. The second-order rate constants given for the quenching reactions of EtOH and TBA are as follows (Li et al., 2018):

$$TBA + OH^{\cdot} \quad 3.8 - 7.6 \times 10^9\ M^{-1}S^{-1} \tag{15}$$

$$TBA + SO_4^{\cdot-} \quad 4.0 - 9.1 \times 10^5\ M^{-1}S^{-1} \tag{16}$$

$$EtOH + OH^{\cdot} \quad 1.2 - 2.8 \times 10^9\ M^{-1}S^{-1} \tag{17}$$

$$EtOH + SO_4^{\cdot-} \quad 1.6 - 7.7 \times 10^7\ M^{-1}S^{-1} \tag{18}$$

Basically, $OH^{\cdot-}$ interacts with targets via hydrogen abstraction, but the $SO_4^{\cdot-}$ response is a precise electron transfer mechanism upon activation.. Hence, $SO_4^{\cdot-}$ is more selective, which is much less of an attractor for TBA. Based on the equations above, it can be observed that $OH^{\cdot}$ appears to be almost 1000 times more reactive than $SO_4^{\cdot-}$ in the reaction rates toward TBA.

3.6.2. Effect of inorganic ions

Natural water usually contains inorganic ions such as HCO_3^-, NO_3^-, $H_2PO_4^-$ and Cl^- which can affect the decomposition of organic compounds by PS radicals in the process of MNC-PS/Fe_3O_4-GO. Previous studies have shown that the presence of some of the involved inorganic ions affects the degradation of organic compounds in sulphate-based advanced oxidation. In this study, the effect of the presence of four types of anions, including HCO_3^-, NO_3^-, $H_2PO_4^-$ and Cl^-, on MT degradation was investigated (Fig. 6-**(B)**). Regarding our results, MT was almost completely degraded (96.5 %) using the PS/Fe_3O_4-GO-MNCs process in the absence of different anions (control), while in the presence of Cl^-, NO_3^-, HCO_3^- and $H_2PO_4^-$ anions, the degradation rate of MT decreased to 84.5 %, 75.2 %, 63.7 % and 56.2 %, respectively, which may be related to the high ionic strength, and the application of PS/Fe_3O_4- further reduced the degradation rate. GO-MNC process. Therefore, the lowest efficiency (56.2 %) is associated with the use of this anion, which may be related to the scavenging properties of $H_2PO_4^-$ for radicals $SO4^{-\bullet}$ and $OH^{\bullet}$. In contrast, H_2PO_4 forms a complex with iron species in the reaction medium, so free cationic iron species have no chance to further react with PS in solution. The degradation rate of MT in the presence of bicarbonate anion was 63.7 % because the presence of bicarbonate in solution resulted in the formation of HCO_3^- and CO_3^{2-} (Eqs. (19) and (20)) (Chai et al., 2021; Lu et al., 2017).

$$H_2CO_3(aq) \rightarrow H^+ + HCO_3^- \tag{19}$$

$$HCO_3^- \rightarrow H^+ + CO_3^{2-} \tag{20}$$

Table 3 Validation of the developed model.

MT concentration (mg/L)	PS dosage (mM)	Fe_3O_4-GO MNCs dosage (mg/L)	Reaction time (min)	Solution pH	Predicted degradation yield (%)	95 % CI low	95 % CI high	Experimental degradation yield (%)
3.7	2.25	225	22	4	95.9	93.3	98.7	96.5
7.2	2.25	225	12.5	4	72.1	69.4	73.6	72.9
3.7	1.30	220	15	4	69.2	69.4	73.8	70.3
5.0	2.0	170	20	4	83.7	81.8	86.5	84.1
6.5	1.5	200	15	4	67.6	65.1	69.5	67.1

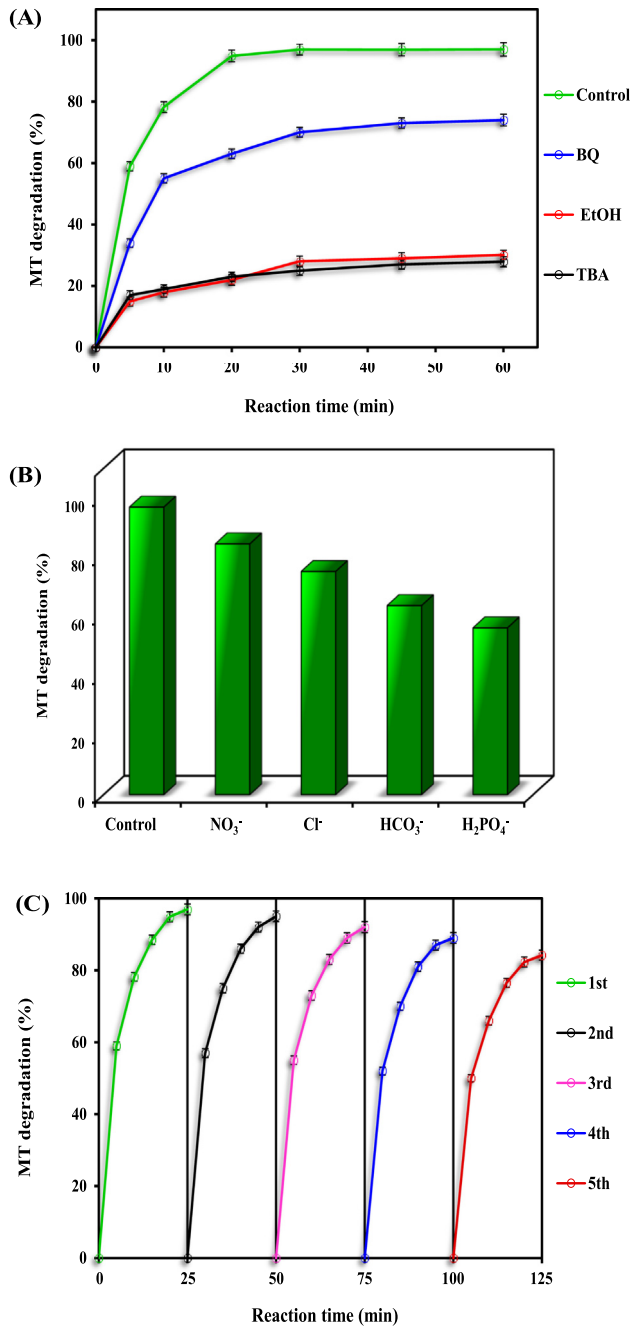

Fig. 6 (**A**) MT degradation yield in the existence of different scavengers, (**B**) Effect of inorganic ions (Inorganic ions concentration of 0.2 mM), (**C**) MT degradation in five cycles in the optimum condition.

On the other hand, $SO_4^{\bullet}$ reacts with HCO_3^- and CO_3^{2-} to form carbonate radicals, which are less capable of decomposing organic pollutants than PS radicals. (Eqs. (21) and (22)).

$$SO_4^{\cdot-} + HCO_3^- \rightarrow SO_4^{2-} + HCO_3^{\cdot} \quad (21)$$

$$SO_4^{\cdot-} + CO_3^{2-} \rightarrow SO_4^{2-} + CO_3^{\cdot-} \quad (22)$$

The effect of bicarbonate inhibition on antipyrine clearance has been reported previously and reached similar conclusions (Chai et al., 2021). Another anion that affects the MT degradation process is chloride. The process results showed that the MT degradation efficiency was 75.2 % in the presence of chloride. Once chloride enters the system, it reacts with $SO_4^{\bullet}$ according to the following equation (Eqs. (23) to (26)) (Fang et al., 2012).

$$SO_4^{\cdot-} + Cl^- \rightarrow SO_4^{2-} + Cl^{\cdot} \quad (23)$$

$$Cl^{\cdot} + Cl^- \rightarrow Cl_2^{\cdot-} \quad (24)$$

$$Cl_2^{\cdot-} + H_2O \rightarrow ClOH^{\cdot} + Cl^- + H^+ \quad (25)$$

$$Cl_2^{\cdot-} + OH^- \rightarrow ClOH^{\cdot} + Cl^- \quad (26)$$

Surface interaction of $SO_4^{\cdot-}$ radicals with Cl^- ions results in the formation of $Cl^{\cdot}Cl^{\cdot}$, which can effectively form other chlorine radicals such as $Cl_2^{\cdot-}$ and $ClOH^{\cdot}$. The production of $Cl^{\cdot}$ can also act in a similar manner to $SO_4^{\cdot-}$ to support the efficient decomposition of pollutants. The results showed that the addition of nitrate reduced MT degradation by about 84.5 %, which may be related to the secondary reaction between nitrate ions and $SO_4^{\cdot-}$ (Eq. (27)) (Zhou et al., 2016).

$$SO_4^{\cdot-} + NO_3^- \rightarrow SO_4^{2-} + NO_3^{\cdot} \quad (27)$$

The above obtained results reveal the influence of inorganic ions on the process. Corresponding to Xu and Li (2010), the HCO_3^-, NO_3^-, $H_2PO_4^-$ and Cl^- ions had a switch effect on the degradation of MT.

Moreover, according to the previous reports, MT degradation can be allocated into two periods, that is degradation and mineralization. MT was attacked by $SO_4^{\cdot-}$ to generate malaoxon and desmethyl malathion. Under further oxidation of $SO_4^{\cdot-}$, they were transformed into different intermediates, such as desmethyl malaoxon, diethyl maleate, diethyl 2-mercaptosuccinate, diethyl malate, ethyl 2-hydroxysuccinate, D-malate, dimethyl phosphate (Li et al., 2019). Finally, the intermediates can be disintegrated into inorganic units through ring-opening and mineralization reactions.

3.7. Reusability of Fe_3O_4-GO MNCs

The reusability potential of the PS/Fe_3O_4-GO MNCs system was investigated in order to determine the practical applicability of the Fe_3O_4-GO MNCs. For this aim, the prepared Fe_3O_4-GO MNCs were used in five subsequent tests and the removal efficiency was recorded. As depicted in Fig. 6-**(C)**, around 13 % decreases in the removal efficiency of MT achieved by the end of the fifth experiment, which demonstrates the appropriate reusability of the Fe_3O_4-GO MNCs in consecutive experiments. This reduction is explained by poisoning the Fe_3O_4-GO MNCs surface with organic by-products or reducing active sites on the catalyst surface.

3.8. Degradation pathway

The proposed degradation pathway of MT demonstrated in Fig. 7 (Li et al., 2019).

3.9. Real sample

The physical and chemical properties of the groundwater samples are shown in Table 5. Treatment trials were performed under most favorable conditions acquired from batch runs. A 100 mL groundwater sample was employed for examination.

The amount of MT remaining in the groundwater samples in this study was determined by solvent extraction experiments with dichloromethane (dichloromethane), which is denser than water (1.33 g mL^{-1}). After filtering the final sample, the solution was transferred to a 1 L decanter, followed by three additional extraction steps using 25, 50, and 25 cm^3 of solvent dichloromethane, respectively. At each stage, transfer the remaining MT to the solvent phase by shaking the decanter. The solvent phase is then drained into a balloon placed underneath. Once the three extraction stages were completed and the solvent phase was completely removed, the indicated amount of anhydrous sodium sulphate was added to the sample to remove water. Thereafter, the separated organic phase was stored in a fume hood and evaporated to fully recover the extraction solvent. After evaporation, a sample volume (500 µL) was set up for analysis on the HPLC system (Dehghani et al., 2017). From the obtained results, it was found that the initial MT concentration of 0.93 ± 0.23 µg.L

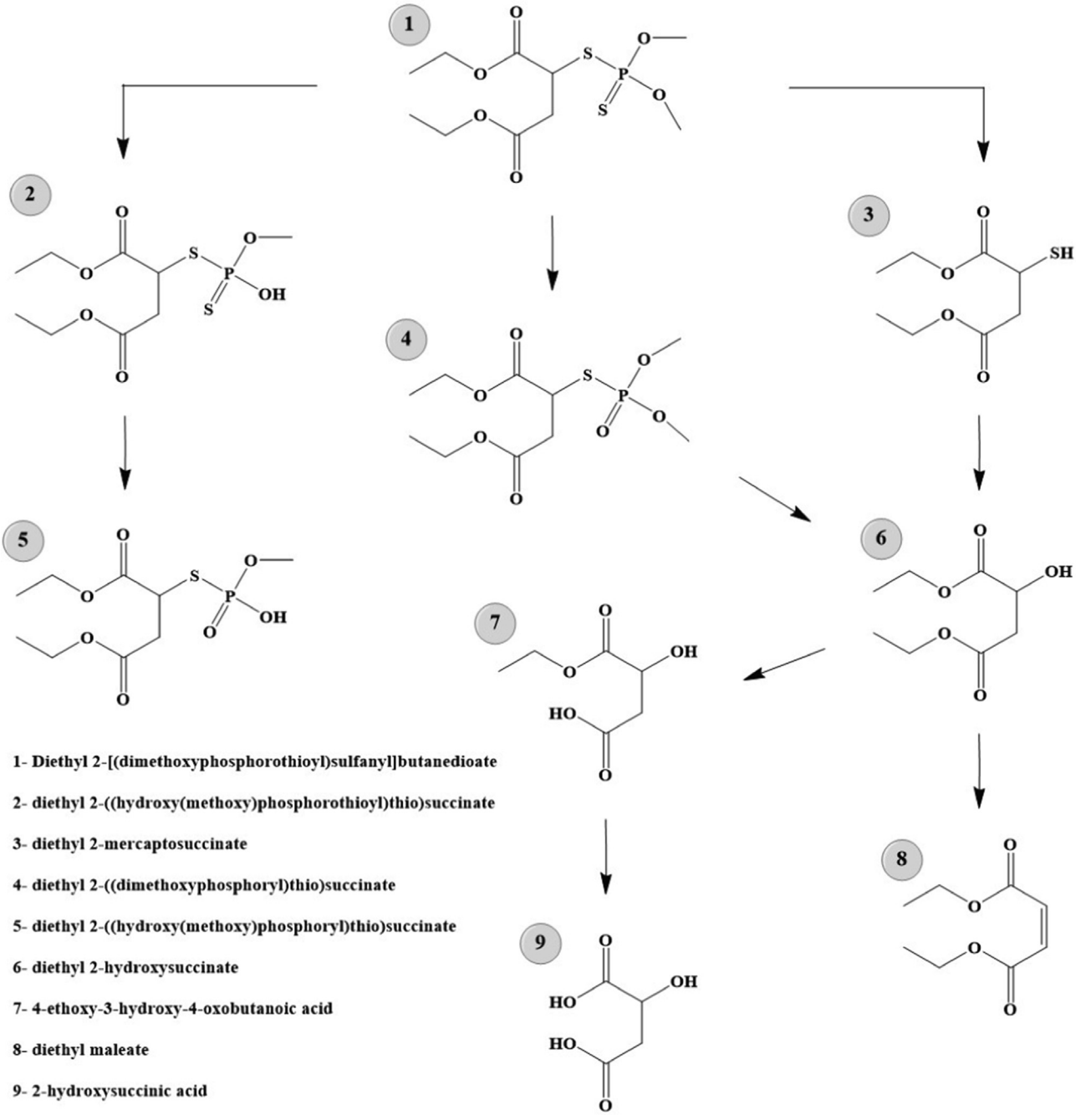

Fig. 7 The proposed degradation pathway of MT demonstrated.

Table 5 Physical and chemical characteristics of groundwater samples.

Parameters	Units	Value
Temperature	°C	20.3 ± 1.5
pH	–	7.62 ± 0.32
EC	μs cm^{-1}	647 ± 35
TDS	mg/L	454 ± 20
Ca^{2+}	mg/L	61.7 ± 13.1
Mg^{2+}	mg/L	12.1 ± 1.1
Fe	mg/L	0.25 ± 0.09
SO_4^{2-}	mg/L	82.4 ± 7.5
NO^{3-}	mg/L	5.1 ± 0.70
Na^+	mg/L	35 ± 4.2
K^+	mg/L	1.26 ± 0.52
F^-	mg/L	0.52 ± 0.12
Fecal Coliforms	CFU 100 mL^{-1}	0
Total Coliforms	CFU 100 mL^{-1}	0

[1] in the groundwater samples decreased to zero under optimal conditions after applying the PS/Fe_3O_4-GO-MNCs method.

4. Conclusion

In this study, the degradation yield of MT by the PS/Fe_3O_4-GO-MNC process was investigated. A four-variable central composite design (CCD) based response surface method (RSM) was used to assess the effect of MT degradation. An analysis of variance was performed to test the validity of the model and a quadratic model was obtained. The MT concentration was 3.7 mg/L, the PS dosage was 2.25 mM, the Fe_3O_4-GO-MNCs dosage was 225 mg/L, the pH was 4, and the reaction time was 22 min. The experimental results show that the MT degradation yield follows a pseudo-first-order kinetic model. $SO_4^{\cdot-}$ performs a major role in MT removal. This mechanism suggests that potentially harmful by-products are not formed or accumulated during MT degradation. Therefore, as a green oxidation process, PS/Fe_3O_4-GO-MNCs have great application potential in the degradation of organic toxic pollutants.

Declaration of Competing Interest

The authors declare that they have no known competing financial interests or personal relationships that could have appeared to influence the work reported in this paper.

Acknowledgements

The authors would like to express their appreciation to Kerman University of Medical Sciences [Grant number 400000699] for supporting the current work.

Funding

This work received a grant from the Kerman University of Medical Sciences [Grant number 400000699].

References

Ai, L., Zhang, C., Chen, Z., 2011. Removal of methylene blue from aqueous solution by a solvothermal-synthesized graphene/magnetite composite. J. Hazard. Mater. 192 (3), 1515–1524.

Amani, A.M., Danaie, P., Vaez, A., Gholizadeh, R., Firuzyar, T., Dehghani, F., Mosleh-Shirazi, S., 2022. Rutin precursor for the synthesis of superparamagnetic $ZnFe_2O_4$ nanoparticles: experimental and density functional theory. Appl. Phys. A 128 (8), 1–10.

Asadzadeh Patehkhor, H., Fattahi, M., Khosravi-Nikou, M., 2021. Synthesis and characterization of ternary chitosan–TiO_2–ZnO over graphene for photocatalytic degradation of tetracycline from pharmaceutical wastewater. Sci. Rep. 11 (1), 1–17.

Bavykina, A., Kolobov, N., Khan, I.S., Bau, J.A., Ramirez, A., Gascon, J., 2020. Metal–organic frameworks in heterogeneous catalysis: recent progress, new trends, and future perspectives. Chem. Rev. 120 (16), 8468–8535.

Borsuah, J.F., Messer, T.L., Snow, D.D., Comfort, S.D., Mittelstet, A. R., 2020. Literature review: global neonicotinoid insecticide occurrence in aquatic environments. Water 12 (12), 3388.

Bray, J.P., O'Reilly-Nugent, A., King, G.K.K., Kaserzon, S., Nichols, S.J., Mac Nally, R., Thompson, R.M., Kefford, B.J., 2021. Can SPEcies At Risk of pesticides (SPEAR) indices detect effects of target stressors among multiple interacting stressors? Sci. Total Environ. 763, 142997.

Carvalho, F.P., 2017. Pesticides, environment, and food safety. Food Energy Secur. 6 (2), 48–60.

Chai, X., Cui, Y., Xu, W., Kong, L., Zuo, Y., Yuan, L., Chen, W., 2021. Degradation of malathion in the solution of acetyl peroxyborate activated by carbonate: products, kinetics and mechanism. J. Hazard. Mater. 407, 124808.

da Costa Filho, B.M., da Silva, V.M., de Oliveira Silva, J., da Hora Machado, A.E., Trovó, A.G., 2016. Coupling coagulation, flocculation and decantation with photo-Fenton process for treatment of industrial wastewater containing fipronil: biodegradability and toxicity assessment. J. Environ. Manage. 174, 71–78.

Dehghani, M.H., Niasar, Z.S., Mehrnia, M.R., Shayeghi, M., Al-Ghouti, M.A., Heibati, B., McKay, G., Yetilmezsoy, K., 2017. Optimizing the removal of organophosphorus pesticide malathion from water using multi-walled carbon nanotubes. Chem. Eng. J. 310, 22–32.

Dehghani, F., Shahmoradi, S., Naghizadeh, M., Firuzyar, T., Vaez, A., Kasaee, S.R., Amani, A.M., Mosleh-Shirazi, S., 2022. Magnetic graphite-ODA@ $CoFe_2O_4$: attempting to produce and characterize the development of an innovative nanocomposite to investigate its antimicrobial properties. Appl. Phys. A 128 (3), 1–13.

DiBartolomeis, M., Kegley, S., Mineau, P., Radford, R., Klein, K., 2019. An assessment of acute insecticide toxicity loading (AITL) of chemical pesticides used on agricultural land in the United States. PLoS ONE 14 (8), e0220029.

Dikshith, T.S.S., Diwan, P.V., 2003. Industrial guide to chemical and drug safety. John Wiley & Sons.

Fang, G.-D., Dionysiou, D.D., Wang, Y., Al-Abed, S.R., Zhou, D.-M., 2012. Sulfate radical-based degradation of polychlorinated biphenyls: effects of chloride ion and reaction kinetics. J. Hazard. Mater. 227, 394–401.

Han, D., Yan, L., Chen, W., Li, W., 2011. Preparation of chitosan/graphene oxide composite film with enhanced mechanical strength in the wet state. Carbohydr. Polym. 83 (2), 653–658.

Hedegaard, M.J., Albrechtsen, H.-J., 2014. Microbial pesticide removal in rapid sand filters for drinking water treatment–potential and kinetics. Water Res. 48, 71–81.

Hussain, I., Zhang, Y., Huang, S., Du, X., 2012. Degradation of p-chloroaniline by persulfate activated with zero-valent iron. Chem. Eng. J. 203, 269–276.

Hussain, I., Li, M., Zhang, Y., Li, Y., Huang, S., Du, X., Liu, G., Hayat, W., Anwar, N., 2017. Insights into the mechanism of persulfate activation with nZVI/BC nanocomposite for the degradation of nonylphenol. Chem. Eng. J. 311, 163–172.

Kassaee, M., Motamedi, E., Majdi, M., 2011. Magnetic Fe_3O_4-graphene oxide/polystyrene: fabrication and characterization of a promising nanocomposite. Chem. Eng. J. 172 (1), 540–549.

Li, N., Tang, S., Rao, Y., Qi, J., Wang, P., Jiang, Y., Huang, H., Gu, J., Yuan, D., 2018. Improved dye removal and simultaneous electricity production in a photocatalytic fuel cell coupling with persulfate activation. Electrochim. Acta 270, 330–338.

Li, W., Zhao, Y., Yan, X., Duan, J., Saint, C.P., Beecham, S., 2019. Transformation pathway and toxicity assessment of malathion in aqueous solution during UV photolysis and photocatalysis. Chemosphere 234, 204–214.

Liang, L., Cheng, L., Zhang, Y., Wang, Q., Wu, Q., Xue, Y., Meng, X., 2020. Efficiency and mechanisms of rhodamine B degradation in Fenton-like systems based on zero-valent iron. RSC Adv. 10 (48), 28509–28515.

Lu, X., Shao, Y., Gao, N., Chen, J., Zhang, Y., Xiang, H., Guo, Y., 2017. Degradation of diclofenac by UV-activated persulfate process: Kinetic studies, degradation pathways and toxicity assessments. Ecotoxicol. Environ. Saf. 141, 139–147.

Luo, H., Gu, Y., Liu, D., Sun, Y., 2021. Advances in oxidative desulfurization of fuel oils over MOFs-based heterogeneous catalysts. Catalysts 11 (12), 1557.

Mahmoodi, H., Fattahi, M., Motevassel, M., 2021. Graphene oxide–chitosan hydrogel for adsorptive removal of diclofenac from aqueous solution: preparation, characterization, kinetic and thermodynamic modelling. RSC Adv. 11 (57), 36289–36304.

Mosleh-Shirazi, S., Kouhbanani, M.A.J., Beheshtkhoo, N., Kasaee, S. R., Jangjou, A., Izadpanah, P., Amani, A.M., 2021. Biosynthesis, simulation, and characterization of $Ag/AgFeO_2$ core–shell nanocomposites for antimicrobial applications. Appl. Phys. A 127 (11), 1–8.

Norzaee, S., Taghavi, M., Djahed, B., Mostafapour, F.K., 2018. Degradation of Penicillin G by heat activated persulfate in aqueous solution. J. Environ. Manage. 215, 316–323.

Popp, J., Pető, K., Nagy, J., 2013. Pesticide productivity and food security. a review. Agro. Sustain. Develop. 33 (1), 243–255.

Rasheed, T., Bilal, M., Nabeel, F., Adeel, M., Iqbal, H.M., 2019. Environmentally-related contaminants of high concern: potential sources and analytical modalities for detection, quantification, and treatment. Environ. Int. 122, 52–66.

Sawinska, Z., Świtek, S., Głowicka-Wołoszyn, R., Kowalczewski, P.Ł., 2020. Agricultural practice in Poland before and after mandatory IPM implementation by the European Union. Sustainability 12 (3), 1107.

Shang, K., Li, W., Wang, X., Lu, N., Jiang, N., Li, J., Wu, Y., 2019. Degradation of p-nitrophenol by DBD plasma/Fe^{2+}/persulfate oxidation process. Sep. Purif. Technol. 218, 106–112.

Sharma, S., Bhattacharya, A., 2017. Drinking water contamination and treatment techniques. Appl. Water Sci. 7 (3), 1043–1067.

Sharma, R.K., Singh, P., Setia, A., Sharma, A.K., 2020. Insecticides and ovarian functions. Environ. Mol. Mutagen 61 (3), 369–392.

Srivastava, A.K., Singh, R.K., Singh, D., 2021. Microbe-based bioreactor system for bioremediation of organic contaminants: present and future perspective. Microbe Mediated Remed. Environ. Contamin. Elsevier, 241–253.

Umar, A.A., Patah, M.F.A., Abnisa, F., Daud, W.M.A.W., 2020. Preparation of magnetized iron oxide grafted on graphene oxide for hyperthermia application. Rev. Chem. Eng.

ur Rahman, H.U., Asghar, W., Nazir, W., Sandhu, M.A., Ahmed, A., Khalid, N., 2021. A comprehensive review on chlorpyrifos toxicity with special reference to endocrine disruption: Evidence of mechanisms, exposures and mitigation strategies. Science of The Total Environment 755, 142649.

Wang, S., Wang, J., Li, C., Xu, Y., Wu, Z., 2021. Ozone treatment pak choi for the removal of malathion and carbosulfan pesticide residues. Food Chem. 337, 127755.

Wu, S., He, H., Li, X., Yang, C., Zeng, G., Wu, B., He, S., Lu, L., 2018. Insights into atrazine degradation by persulfate activation using composite of nanoscale zero-valent iron and graphene: performances and mechanisms. Chem. Eng. J. 341, 126–136.

Yao, Y., Miao, S., Liu, S., Ma, L.P., Sun, H., Wang, S., 2012. Synthesis, characterization, and adsorption properties of magnetic Fe_3O_4@ graphene nanocomposite. Chem. Eng. J. 184, 326–332.

Zaaba, N., Foo, K., Hashim, U., Tan, S., Liu, W.-W., Voon, C., 2017. Synthesis of graphene oxide using modified hummers method: solvent influence. Procedia Eng. 184, 469–477.

Zhen, G., Lu, X., Su, L., Kobayashi, T., Kumar, G., Zhou, T., Xu, K., Li, Y.-Y., Zhu, X., Zhao, Y., 2018. Unraveling the catalyzing behaviors of different iron species (Fe^{2+} vs. Fe0) in activating persulfate-based oxidation process with implications to waste activated sludge dewaterability. Water Res. 134, 101–114.

Zhou, T., Zou, X., Mao, J., Wu, X., 2016. Decomposition of sulfadiazine in a sonochemical Fe0-catalyzed persulfate system: parameters optimizing and interferences of wastewater matrix. Appl. Catal. B: Environ. 185, 31–41.